Solvent-dependent Photo-induced Dynamics in a Non-rigidly Linked Zinc Phthalocyanine-Perylenediimide Dyad Probed by Ultrafast Spectroscopy

Bryan Kudisch[1], Margherita Maiuri[1], Vicente M. Blas-Ferrando[2], Javier Ortiz[2], Ángela Sastre-Santos[2], Gregory D. Scholes[1]

[1]Department of Chemistry, Princeton University, Princeton, NJ, 08540, United States

[2]Área de Química Orgánica, Instituto de Bioingeniería, Universidad Miguel Hernández, Elche 03202, Spain

gscholes@princeton.edu , asastre@umh.es

Abstract: In this work, we characterize the energy and electron transfer kinetics of a zinc phthalocyanine-perylenediimide dyad (ZnPc-PDI) in various solvents using steady-state and tunable narrowband pump-probe spectroscopy. We fit the ultrafast data with global analysis techniques and find that upon excitation of the PDI moiety, (pump pulse at 540 nm) the excitation energy transfer (EET) rate to the ZnPc moiety displays a solvent sensitivity that we attribute to changes in relative equilibrium moiety orientation. We rationalized these observation by considering the nature of the non-rigid bridge used to link the two moieties as well as the degenerate nature of the Q band transitions in the ZnPc species. When we tuned the pulse in resonant with the ZnPc moiety (685 nm) we directly photo-induce an electron-transfer process back to the PDI. Employing the same global analysis, we find that the dynamics of the ultrafast electron transfer (ET) are completely kinetically controlled according to the Bixon-Jortner model of barrierless solvent-controlled curve crossing, while the recombination to reform the ground state is well-described by the static energetic picture according to Marcus theory.

1. Introduction

Molecular model systems have been increasingly developed to predict and understand the photophysical behavior of both natural and artificial light harvesting systems[1-4]. In the framework of renewable energy technologies such as organic photovoltaics (OPVs), model systems composed of carbon-based chromophores have been designed in order to better understand which steps in the energy conversion process could be responsible for low overall efficiency, and thus subsequently optimized for better device performance[5-6]. Donor-acceptor (D-A) dyad systems in solution have been extensively studied to investigate myriad fundamental photophysical processes at play in both functional organic electronics and natural light induced processes, with particular emphasis on excitation energy transfer (EET) and charge transfer with great contextual diversity[7-12].

Two particularly commonly used molecular moieties for model systems are the zinc phthalocyanine (ZnPc)[13-14] and the perylenediimide (PDI) [14,15] . These planar molecules contain delocalized π-electron systems leading to strong absorption in the visible region of the electromagnetic spectrum[16-17]. Along with their high extinction coefficients, both the perylene and phthalocyanine classes of molecules are remarkably photostable and make for easy solution processing either for use in devices[18-19], or as dyes for painting applications[20]. D-A type molecular systems composed of PDIs and Pcs have shown a variety of photophysical dynamics following photoexcitation, both in mechanism and in reaction kinetics[21-24].

Here we study a ZnPc-PDI dyad[25] by ultrafast pump-probe spectroscopy. In this model system, the ZnPc is linked via a peripheral position ethoxy bridge at the imide site of the PDI, shown in Figure 1. The lack of conjugation and the length of the ethoxy bridge points to a weakly coupled D-A molecular system such that the absorption spectrum of the dyad is similar to the sum of the absorption spectra of the two components[25-26]. Furthermore, two sulfone groups have been added to the PDI 1,7-bay positions, and six tert-octylphenoxy groups to the peripheral positions of the ZnPc, which alter the relative energies of the excited states of the molecules without changing the overall electronic structures of the ground state[15, 27]. The photophysics upon excitation at 355, 410, and 530 nm of this ZnPc-PDI dyad have been previously studied in toluene and benzonitrile (PhCN), where the authors reported EET from PDI to ZnPc and photoinduced electron transfer (ET) from ZnPc to PDI on the femtosecond and picosecond timescales[28].

Our investigation aims to complement previous studies of the excited state dynamical processes in the ZnPc-PDI system by tracking kinetics changes upon solvent variation. We employ two sets of experiments where the excitation wavelength is tuned either to the PDI or ZnPc lowest excited singlet state, 540 nm and 685 nm respectively. The chosen solvents are toluene, PhCN, tetrahydrofuran (THF), and dichloromethane (DCM), which have different properties in terms of size, dielectric constant (ε), and dielectric relaxation time (τ_d). These key parameters represent the main factors that have been shown to influence photodynamic kinetics and mechanisms according to the Bixton-Jortner and Marcus models for electron transfer as well as the weak-coupling Förster resonance energy transfer model [29-30]. Recently, others have shown a solvent dependence to

electron transfer in similar ZnPc-PDI systems[31-32]—our experiments serve to complement their results with a physical description of the origin of the ultrafast kinetics and steady-state spectral features. We find that the differences in EET rates between our dyad in different solvents are more readily explained by a flexibility in moiety arrangement which modifies the center-to-center distance between the moieties. Furthermore, we find that by varying the solvent we elucidate the mechanism of both the forward and back ET, as the forward ET appears to trend with the dielectric relaxation time of the solvent even though the reaction should classically be in the Marcus inverted region in all solvents, while the rate of back ET is completely controlled by the energetics of the charge-separated state and spans from the normal to inverted Marcus regimes.

2. Experimental methods

Perylene monoimide monoanhydride (PMAMI), ZnPc, and ZnPc-PDI were synthesized according to the procedure in Ref. 25, and then used as received. Steady-state absorption measurements were taken using an Agilent Cary 60 Spectrophotometer (Agilent Techonologies, Santa Clara, CA), with an integration time of 0.1 s and a data interval of 1 nm. Fluorescence measurements were taken using a QuantaMaster 400 (HORIBA Scientific, NJ), with excitation and emission slit widths of 2 nm. The emission monochromator which was used for PMAMI fluorescence measurements utilizes a grating with 1200 lines/mm and is blazed for 400 nm, while the ZnPc fluorescence measurements the monochromator was changed to a grating with 600 lines/mm and blazed for 1000 nm. Absorption measurements were done using a 1 mm cuvette, for which the maximum absorbance for the measured solution was never above 0.1 OD. For the fluorescence measurements, a 1 cm cuvette was used and the OD was never above 0.05 OD in order to avoid inner filter effects.

The full description of the pump-probe setup can be found elsewhere[33]. Briefly, a 1 kHz regeneratively amplified Ti:sapphire laser system (Coherent Libra, Santa Clara, California) outputs approximately 45 fs pulses centered at 800 nm with an average power of 4 W. The beam is sent through a 90-10 beamsplitter to create pump and probe arms. The pump arm takes higher power reflected pulses and directs them into a commercial optical parametric amplifier (OPerA Solo, Vilnius, Lithuania), which converts the input 800 nm pulses into narrowband (~10 nm) temporally short (100 fs) pulses at either 540 or 685 nm. Both the output of the OPerA Solo along with the remainder of the Coherent Libra output from the beamsplitter were directed into a commercial transient absorption spectrometer (Ultrafast Systems Helios, Sarasota, Florida). The pump light was sent through a 500 Hz optical chopper and then focused into a 1 mm cuvette containing the sample at 0.1 OD, with an incident pump power of 125 μW. A power dependent study on all samples can be found in the Supplementary Information. We found that the 125 μW pump power is within the linear excitation regime for each molecule studied with the exception of ZnPc. In order to fulfill the linear excitation criterion for this sample, Fig. 2b shows the transient spectra of ZnPc measured at 60 μW pump rower. The probe pulse is generated by focusing the 800 nm pulses into a sapphire crystal, producing a supercontinuum from 450 nm to 800 nm. The residual fundamental from the supercontinuum generation was minimized using optical filters, and

the probe light was spatially overlapped with that of the pump and focused onto the cuvette. The spectral difference between the transmission of the probe pulse through the sample with and without the pump pulse constitutes a ΔA signal according to:

$$\Delta A(\lambda, t) = -\log\left(\frac{T_{pump\ on}(\lambda, t)}{T_{pump\ off}(\lambda)}\right)$$

Combinations of λ/2 waveplates and polarizers were used to both attenuate the beams as well as to control the polarization of the incident light. The relative polarization of the pump pulse to the probe pulse for the measurements was 54.7°. Pump-probe temporal delays were achieved by delaying the probe arm before supercontinuum generation, which were exponential in terms of temporal spacing from short times to long times. Each scan contained up to 1000 points, and >20 scans were averaged in order to increase the signal-to-noise ratio. The resultant transient absorption spectra were also corrected for group velocity dispersion by polynomial fitting of the coherent artifact.

For this study, ZnPc-PDI in all four solvents were analyzed using global analysis[34]. Software to perform this kind of analysis is freely available using the Glotaran software package, which allows specification of a particular kinetic scheme as well as the number of states to model the kinetic evolution of the transient spectra[35]. For this analysis, we use only use the time points in the experiment after the coherent artifact and submit to the analysis software a near delta function width for the instrument response function (IRF). For the 540 nm excitation wavelength, we limit our analysis to only the first 3 ps after photoexcitation, since the subsequent dynamics is essentially equivalent to the experiment with 685 nm excitation, although with lower signal-to-noise due to the lower extinction coefficient at 540 nm. For the 685 nm excitation wavelength, we impose a sequential population model, meaning that there is an evolution-associated decay spectrum (EADS) which corresponds to each of the states that decay into each other with rate constants that minimize the residual between the data and the global fit. In essence, each of these states has its own associated transient spectrum which evolves into the subsequent state with its own spectrum, an evolution which occurs with a particular rate k_i which denotes the evolution from state *i* to state *i-1*. Evolution of EADS is a much more reliable metric for dynamics than single wavelength traces, since the evolution of one spectrum to another accounts for shifts in peak positions as well as overall amplitude changes in the spectrum.

3. Results

A. Steady-state absorption and fluorescence of constituent monomers. The steady-state absorption spectrum of PMAMI in toluene is reported as the solid red trace in Figure 1a, depicting the characteristic vibronic progression associated with the perylene family of molecules. The λ_{max} of PMAMI in toluene is centered at 523 nm (19,100 cm^{-1}) and corresponds to the 0-0 vibronic peak of the S_1 transition. As is the case for most substituted perylenes and perylene derivatives,

the transition dipole moment of the S_1 transition in PMAMI points along the long molecular axis[36]. The fluorescence spectrum upon excitation at 475 nm is reported as the dotted red trace in Figure 1a.

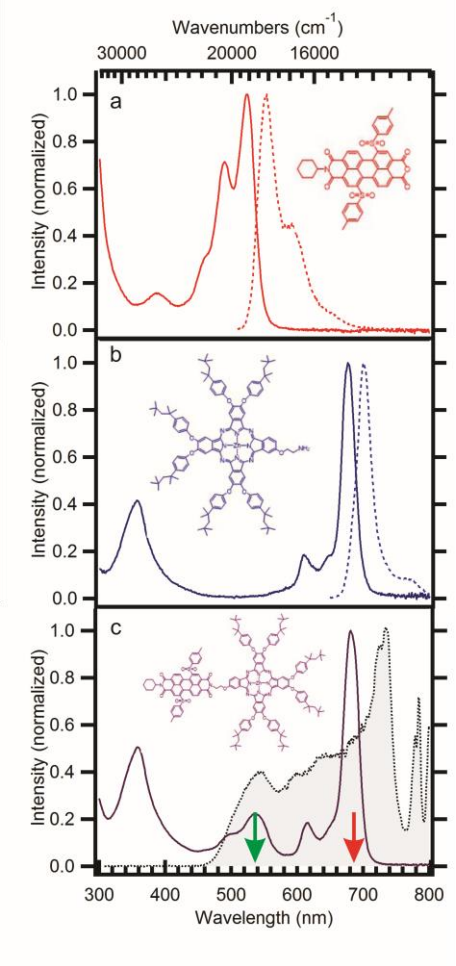

Figure 1. Absorption and fluorescence spectra of (a) PMAMI (b) ZnPc (c) ZnPc-PDI, as well as the probe spectral coverage (shaded) and the pump wavelengths (540 nm green, 685 nm red arrows)

The λ_{max} for fluorescence in PMAMI is at 552 nm (18100 cm^{-1}), corresponding to a Stokes shift of 1,000 cm^{-1}. The fluorescence quantum yield for PMAMI and related perylenes have been shown to be greater than 90%, corresponding to relatively slow rates of intersystem crossing and nonradiative decay in comparison to the rate of the fluorescence[37]. Due to the two sulfone groups attached to the bay positions of the perylene core, heavy atom effects increase the spin-orbit coupling, consequentially increasing the rate of intersystem crossing and decreasing the fluorescence quantum yield in comparison to more standard perylene derivatives. They also serve to spread out the electron density further from the core of the molecule, a substitution which is known to further stabilize the perylene anion.

The steady-state absorption spectrum of ZnPc in toluene is reported as the solid blue trace in Figure 1b. As a member of the metal phthalocyanine family, the absorption spectrum is characterized by a strong absorption at 676 nm (14,800 cm^{-1}), which in metallated systems denotes the Q (0-0) transition. Two vibronic shoulders Q (0-1) and Q (0-2) peak are located at 645 nm and 610 nm respectively. The Q transition in metallated and symmetric phthalocyanines is composed of two degenerate perpendicular transition dipole moments that point from each pyrrole ring to the one in the opposite corner. The broad peak centered at 357 nm is assigned to the Soret transition, denoted the B band, although computational studies[38] as well as magnetic circular dichroism[39] support the hypothesis of a manifold of electronic transitions. The fluorescence spectrum upon excitation at 620 nm reported as the dotted blue trace in figure 1b, displaying a λ_{max} of fluorescence at 701 nm (14,300 cm^{-1}) and corresponding to a Stokes shift of 500 cm^{-1}. Fluorescence quantum yields for metallated phthalocyanines usually depend on the extent of spin-orbit coupling, which correlates with the molecular weight of the coordinating metal. Because of the competition between the nonradiative decay, intersystem crossing, and fluorescence decay, the fluorescence quantum yield for our ZnPc should be ~10%[40].

The steady-state absorption spectrum of ZnPc-PDI, reported in Figure 1c, is clearly comprised of a linear combination of the PMAMI and the ZnPc absorption spectra. However, some differences can be noted: the spectral features related to the ZnPc at 358 nm and 681 nm are are both redshifted from the original monomer absorption. Furthermore, the ratio of oscillator strength between these two peaks has changed, with the B transition appearing with relatively greater intensity when both ZnPc and ZnPc-PDI are normalized at the Q(0-0) transition. The Q transition region shows further changes in the dyad as compared to ZnPc, where the Q(0-1) shoulder seems to lose oscillator strength to the point where it is no longer clearly visible, while the Q(0-2) feature does not noticeably change aside from the aforementioned redshift. The transitions between 450 and 580 nm in ZnPc-PDI mostly resemble PMAMI absorption features, with the absorption maximum in this region red-shifting to 536 nm along with spectral broadening of its vibronic features. Both the 0-2 vibronic transition in the S_1 vibronic manifold and the S_2 transition in the PMAMI cannot be identified in the dyad, likely due to the underlying absorption coming from the lower energy tail of the B transitions in the phthalocyanine. A similar tail in the Q region absorption can be seen overlapping slightly with the redmost portion of the now PDI moiety absorption. Previous studies on this ZnPc-PDI dyad report a fluorescence quantum yield decrease of 97% going from the ZnPc monomer to the ZnPc-PDI dyad[28]. The lack of appearance of any new absorption features, as well as the retention of the individual features of the PDI and ZnPc moieties point to a weak coupling between the two constituent chromophores in the dyad.

B. Excitation energy transfer (EET) from PDI* to ZnPc in toluene. The ultrafast transient absorption spectra ΔA of PMAMI in toluene upon photoexcitation at 540 nm are shown in Figure 2a at different pump-probe delays. At the earliest time (0.1 ps), after the contribution from the coherent artifact, the spectrum is dominated on the blue side of the spectrum with negative ΔA signal, corresponding to a mixture of ground state bleaching (GSB) and stimulated emission

(SE), and in the red side of the spectrum, a positive ΔA signal which denotes an excited state absorption (ESA). The three negative peaks on the blue side of the pump-probe spectrum correspond to the three peaks in the absorption spectrum, hence designating a mixture of SE and GSB features. The ESA centered at 746 nm corresponds to a S_1 to S_n transition, where S_n is a higher lying singlet excited state[36]. At 5 ns, we notice that all pump-probe signals from the PMAMI have mostly decayed, in agreement with nanosecond fluorescence lifetime measurements[41].

Figure 2b shows the transient absorption spectra of ZnPc in toluene measured at different pump-probe delays after photoexcitation at 685 nm. At 0.2 ps after photoexcitation, the spectrum displays multiple ESA features, some of which overlap the negative pump-probe signals between 600 and 720 nm. The most prominent negative feature at 696 nm is attributed to a mixture of GSB and SE, which is located energetically intermediate between the absorption and fluorescence maxima. At 100 ps after photoexcitation, we note little to no change in the pump-probe spectrum, suggesting that any dynamics in the system is occurring on a slower timescale than in the hundreds of picoseconds, which agrees well with earlier studies of a similar zinc phthalocyanine[41]. At 5 ns, we observe a substantial decay of the mixed SE and GSB feature at 697 nm as well as a decay of ESA signal centered at 700nm and extending toward the NIR region. We attribute the decay of the ESA to the formation of the triplet excited state, $ZnPc^3$, which is known to have a broad ESA feature centered at 520 nm. The partial decay of the GSB on this timescale implies an intersystem crossing rate which is similar in magnitude to the rate of nonradiative population recovery to the ground state[41].

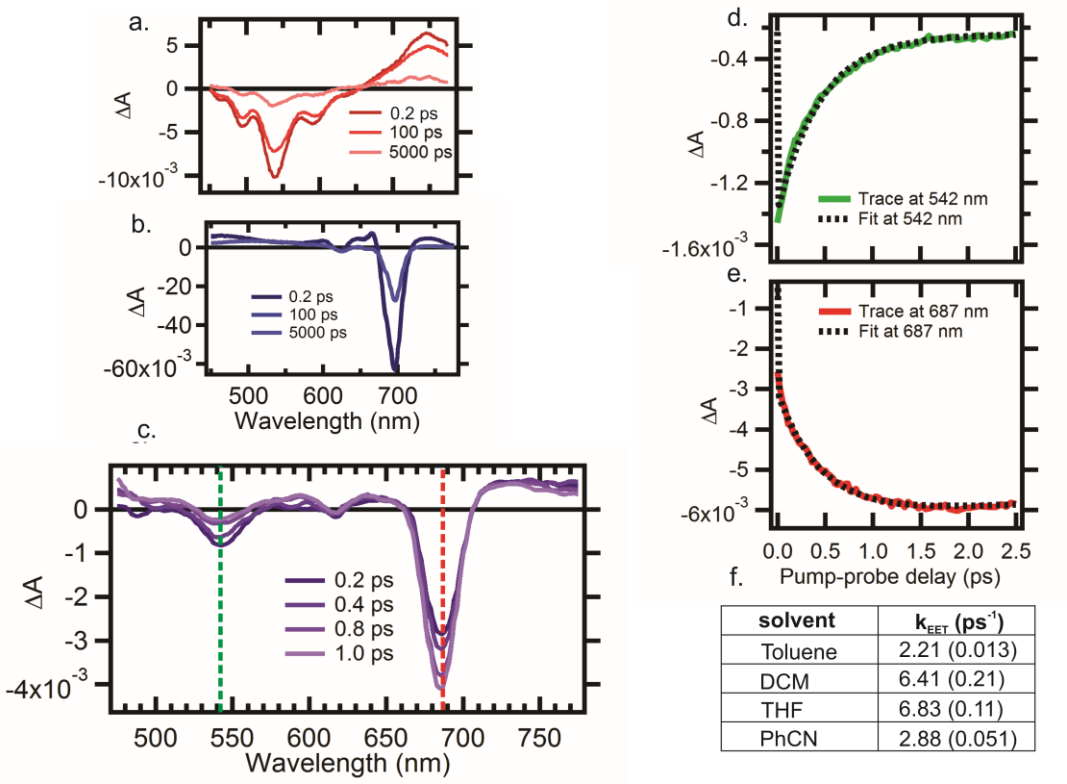

solvent	k_{EET} (ps^{-1})
Toluene	2.21 (0.013)
DCM	6.41 (0.21)
THF	6.83 (0.11)
PhCN	2.88 (0.051)

Figure 2. Pump-probe spectra of PMAMI (a) and ZnPc (b) after photoexcitation at 540 nm and 685 nm respectively at various pump-probe delay (c) Transient spectra of ZnPc-PDI following photoexcitation at 540 nm, with traces from this experiment at (d) 542 nm and (e) 687 nm shown with global analysis fits. (f) Table of rate constants for EET extracted from global analysis, where the numbers in parentheses are the errors to that decay component in the fit. All measurements were performed at 125 μW pump power, with the exception of the ZnPc experiment, which was performed at 60 μW.

Upon photoexcitation of the ZnPc-PDI dyad at 540 nm (Fig. 2c), we detect spectral features that correspond to a combination of the individual signals observed in the transient spectra of the individual moieties. Specifically, 0.2 ps after photoexcitation the SE and GSB bands of both the PDI and ZnPc chromophores are present, as well as a broad ESA which extends from 625 nm to the red edge of our detection range. With increasing pump-probe delay, we see the decrease of the SE feature in the PDI region concomitant with the increase of both the SE band in the region attributed to ZnPc and of the ESA features at shorter wavelengths. The kinetic traces in the PDI and ZnPc SE regions are shown in Figures 2d and 2e, respectively. The ESA at higher wavelengths remains relatively unchanged on this timescale, due to the overlapping of the two separate ESA bands from PDI and ZnPc which leads to an apparent negligible change in intensity in this spectral region for the dyad. It should be noted that following the transfer of population from the PDI moiety to the ZnPc moiety, we only observed a growth in the negative signal in the ZnPc bleach region without red-shifting of the peak to the new maximum of the GSB and SE combined negative feature. The lack of observation of this red-shifting is likely due to the simultaneous growth of the ZnPc S1 ESA signal which largely overlaps with the red side of the GSB and SE signals, which may obscure this spectral evolution.

As shown in S19-S21, we observe multiexponential decay kinetics in the ZnPc SE feature on the picosecond timescale following the end of its growth, as well as convoluted evolution kinetics in the ESA regions both immediately to the red of this region as well as at the highest energy edge of our detection limit. Assuming that these dynamics are the result of the population of the S_1 of the ZnPc moiety due to energy transfer, as we will discuss in the Discussion section, we investigate these dynamics by directly exciting the ZnPc moiety at 685 nm. Since the extinction coefficient at this wavelength relative to that at 540 nm is much greater, investigation of the subsequent dynamics at this wavelength affords much greater signal to noise, as well as less convolution of dynamics that may stem from PMAMI monomer impurities in the ZnPc-PDI solution.

D. Electron transfer from ZnPc* to PDI in toluene. Upon photoexcitation of the ZnPc-PDI dyad at 685 nm (Fig. 3a), we again observe a combination of features belonging to the individual moieties. At 0.2 ps after photoexcitation, the pump-probe spectrum looks quite similar to the spectrum after excitation at 540 nm, with a few important exceptions. The main difference arises when we look at the negative pump-probe features, where the ZnPc SE feature is the most intense negative feature, accompanied by ESA features which correspond to a ZnPc population of

the Q state. The negative pump-probe signal in the PDI region of the spectrum is notably less intense than in the 540 nm excitation case when compared to the negative signal in the ZnPc region, further corresponding to a population of mainly the ZnPc S_1 state.

The spectral progression from 0.2 ps to 10 ps displays some relatively surprising dynamical signatures. The negative features ascribed to the combined SE and GSB of the Q band of the ZnPc appears to both decay and blue-shift, accompanied by a growth and blueshift of the ESA located in the 730 nm region. Upon progressing to 100 ps after photoexcitation, we report a global decrease in intensity for both negative and positive pump-probe features.

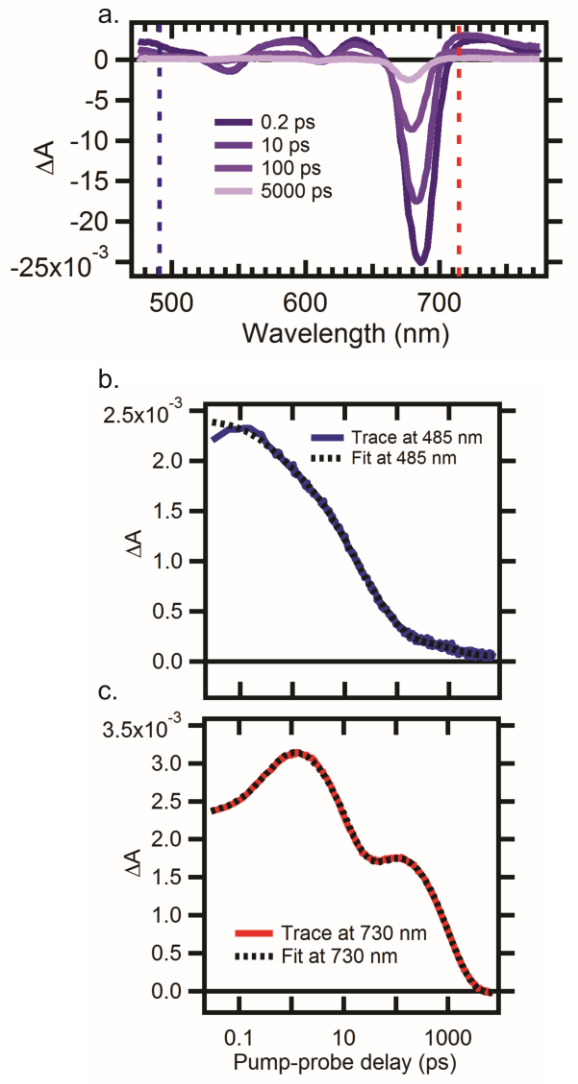

Figure 3. a. Pump-probe spectrum of ZnPc-PDI upon photoexcitation at 685 nm from 0.2 ps to 5000 ps b. Kinetic trace at 485 nm after 685 nm photoexcitation c. Kinetic trace 730 nm upon photoexcitation at 685 nm.

E. Solvent-dependent dynamics of ZnPc-PDI. We investigated the solvent effects on these photoinduced dynamics upon photoexcitation of ZnPc-PDI by comparing the transient absorption data of ZnPc-PDI measured in toluene with similar measurements of the dyad in THF, DCM, and PhCN. The absorption spectra of the ZnPc-PDI in various solvents are shown in the supplementary information (S7-9), and we note that there are not significant differences in the absorption spectra, despite some minor solvatochromic shifts in both the PDI and ZnPc regions. Furthermore, the excited state dynamics of our molecule in these different solvents display the similar overall dynamics, although with different kinetics, as displayed in Figure 4. The top traces in Figure 4a report the decay of the negative transient signal at 542 nm for all four solvents. In DCM and THF, the intensity of the signal decreases much faster than in the case of Tol and PhCN. Just as in the case of toluene, the early timescale population dynamics appear easy to analyze by looking at the GSB and SE region for the ZnPc moiety at 687nm, reported as the bottom traces in figure 4a. Predictably, this negative feature grows fastest for the DCM and THF cases.

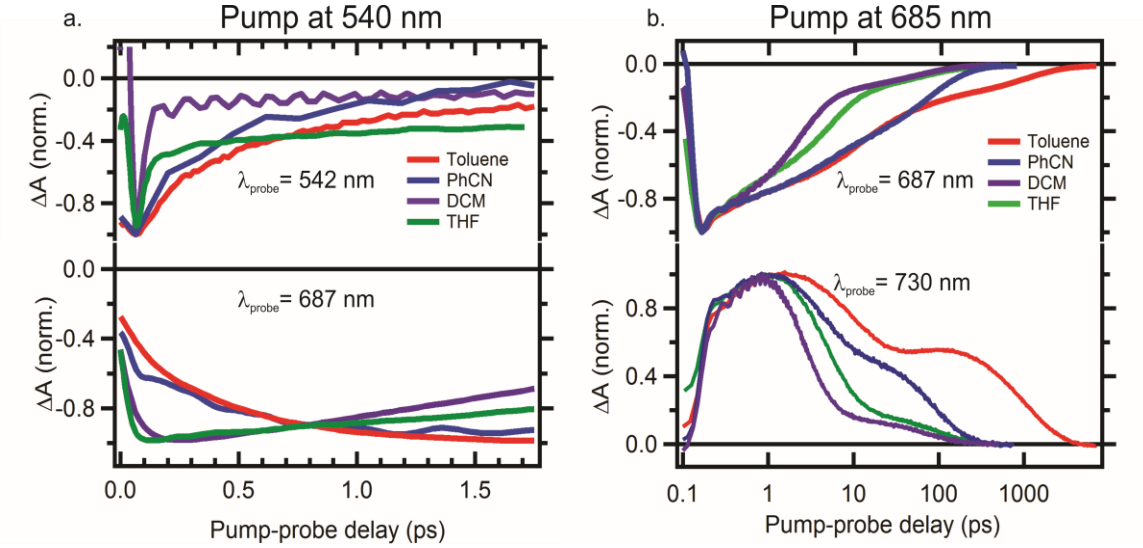

Figure 4. (a) Traces displaying population dynamics at early times following photoexcitation at 540 nm and with probe wavelength at 542 nm (top) and 687 nm (bottom) corresponding to energy transfer in different solvents. (b) Traces displaying population dynamics following photoexcitation at 685 nm and with probe wavelength at 687 nm (top) and 730 nm (bottom).

Figure 4b shows the solvent dependence upon photoexcitation at 685 nm. We start from the traces reflecting the decay of the ZnPc SE (top traces of figure 4b). Similar trends are observed in the two probe temporal delays in THF and DCM (0.2 ps to 1-2 ps) and in toluene and PhCN (0.2 ps to 5-10 ps). While others have attributed the initial dynamics after photoexcitation to solvent relaxation[41-42] (an explanation which also our results support) the similarities between these initial dynamics of our dyad in PhCN and toluene is unexpected. The dynamical decrease in intensity of the SE following this initial event, though, in general displays biexponential character, which is relatively unsurprising considering that we are aware of the overlap of GSB and SE features from the ZnPc moiety. This picture becomes more complicated in the case of toluene,

where not only the duration of the excited state is much longer than that of others, but that also the decay of the SE and GSB follows a clear multi exponential trend. This picture becomes obvious as we analyze the traces at 730 nm for the various solvents, (bottom Figure 4b bottom panel). In toluene, the perplexing kinetics which was hinted at in tracking the SE manifests itself in the form of a decay in ESA signal, then subsequent rise in signal presumably after the population transfer has completed from ZnPc*, and finally a resumption of the decay of this signal on a much longer timescale than in DCM, THF, and PhCN.

4. Discussion

A. Solvent-dependent EET dynamics. The extracted rate constants upon photoexcitation at 540 nm are reported in Figure 2f. We constrain the fitting procedure up to 3ps in all cases, which correspond to the energy transfer time from the PDI to the ZnPc before the ZnPc starts to decay. We use the Förster resonance energy transfer model to interpret the experimental rates:

$$k^{Förster} = \frac{\frac{1}{\tau_D} 9 \ln(10) \kappa^2 \varphi_D J}{128 \pi^5 N_A n^4} \frac{1}{R^6} \quad (1)$$

Where τ_D is the lifetime of the donor moiety, κ is the orientation factor of the donor and acceptor transition dipole moments, J is the spectral overlap between the normalized fluorescence spectrum of the PDI donor and the extinction spectrum of the ZnPc acceptor, n is the bulk index of refraction of the medium, and R is the center-to-center distance between the donor and acceptor in cm[43]. Generally, we consider that solvents mainly modify the index of refraction (where increasing the index of refraction decreases the rate of energy transfer due to screening effects). Nevertheless, in our case changing solvents from toluene (n = 1.50), to DCM and THF (n = 1.41 and 1.42, respectively) increases the rate (2.21 to 6.41 and 6.83 ps^{-1}) close to threefold. A similar inconsistency with the Förster rate arises when we consider that the energy transfer in PhCN (n = 1.53) is faster (2.88 ps^{-1}) than in toluene, even if we should expect a slower rate strictly from a dielectric constant consideration.

The hypothesis that changes in the orientation factor and/or change in the center-to-center distance between the two chromophores are responsible of the anomalous trend in the energy transfer rate seems more plausible. The PDI and ZnPc moieties are linked together by a non-sterically bulky aliphatic linker, as opposed to a rigid linker, linkers which are commonly used in the field of model systems to restrict variations in chromophore nuclear conformation. A non-rigid linker or bridge between two coupled moieties usually implies some conformational freedom in the dyad, despite the relatively large amount of steric bulk attached to both PDI and ZnPc moieties. Such conformational freedom could vary both the orientation factor and the center-to-center distance about the equilibrium position, with the consequence of broadening the steady-state absorption features of the dyad with respect to the individual monomers, which is more clearly seen in the linear absorption measurement where the PDI moiety absorbs. In our dyad system, we note that the ZnPc acceptor has two degenerate and orthogonal transition dipoles, one of which is on the axis where the moieties are covalently bound. These degenerate transition dipoles in the Q

band differ in their orientation, so the Förster equation needs to account for two possible acceptor transitions:

$$k_{EET} \sim \frac{\kappa^2}{R^6} \rightarrow k_{EET} \sim \frac{\kappa_{tot}^2}{R^6} = \frac{\kappa_1^2+\kappa_2^2}{R^6} \quad (4)$$

A detailed treatment of the implications of both the non-rigid linker of the PDI and ZnPc moieties is given in the Supplementary Information (S22). If we consider variability in the arrangement of transition dipole moments with the assumption that they are all coplanar, we note that the value of $\kappa_1^2 + \kappa_2^2$ deviates from the maximum value of 4 to ~2.5 at an angle of $\frac{\pi}{2}$ radians between the donor and the acceptor transition dipole moment parallel to the linker. Thus, if we consider the progression away from linearity in the case of the two transition dipoles acceptors, we recover a scenario where κ_{tot}^2 remains relatively constant in comparison to large increases of the value of $1/R^6$, corresponding to an increased sensitivity of the EET rate to the nuclear configurations of the chromophores. The sensitivity in the relative orientation of the PDI and ZnPc chromophore transition dipole moments could explain the drastic differences in the EET rates despite similar spectroscopic factors as the spectral overlap and indices of refraction for the various solvent cases.

B. Solvent-dependent photoinduced ET. Table 1 reports the extracted decay rate constants after photoexciting the system at 685 nm. We have considered the full decay evolution up to the nanosecond time scale and fit the decay evolution with 6 EADS which is the minimum number of significant spectra needed. Global analysis with 5 EADS are reported in the supplementary, along with the residuals associated with the fits of both the 5 and 6 EADS models (Figures S23-S40). Figure 5 shows the EADS spectra obtained by global analysis in different solvents in the 500-720 nm range.

Table 1. Rate constants for the spectral evolution of ZnPc-PDI in different solvents.

	decay rate constants (ps^{-1})					
solvent (pump 685nm)	k_1	k_2	k_3	k_4	k_5	k_6
Toluene	2.7 (0.03)	0.47 (0.005)	0.09 (0.001)	0.016 (0.0001)	0.0009 (0.00001)	0.00005 (7E-6)
Amplitude	0.924	0.691	0.677	0.688	0.835	0.847
THF	2.77 (0.006)	0.23 (0.0027)	0.26 (0.003)	0.037 (0.0003)	0.0096 (0.00005)	0.0002 (0.00006)
Amplitude	0.984	0.801	0.344	0.647	0.619	0.909
DCM	2.08 (0.009)	0.4 (0.02)	0.39 (0.02)	0.051 (0.0008)	0.014 (0.0001)	0.00006 (0.0002)
Amplitude	0.999	0.672	0.369	0.679	0.618	0.975

PhCN	2.2 (0.03)	0.51 (0.009)	0.21 (0.005)	0.033 (0.0008)	0.017 (0.0005)	0.004 (0.00009)
Amplitude	0.947	0.645	0.529	0.695	0.488	0.615

Table of rates derived from global analysis, employing a kinetic scheme with 6 levels and 6 rates for each solvent. Numbers in parentheses are the errors associated with each rate constant. Amplitudes are reported as the maximum value attained by the associated EADS such that the sum of each EADS at any point in time is equal to 1.

We observe a decrease in amplitude of the ZnPc SE as well as a changing ESA profile which corresponds to the deactivation of the ZnPc-PDI* excited state as it undergoes electron transfer to form $ZnPc^{+}$-PDI^{-}, which is reflected in toluene and PhCN as the decay of the 3rd EADS (EADS3) to EADS4. The evolution from EADS1 to EADS3 within these solvents is characterized by spectral shifts in the ESA and SE peaks as well as minor changes in amplitude of these features, the amplitude changes most likely deriving from the overlapping of positive and negative transient signals. These spectral evolutions can be interpreted within the framework of previously reported ultrafast kinetics in zinc phthalocyanines that can come from dielectric solvent responses to the new charge distribution of the solvated dyad, although we are also unable to rule out contributions from ultrafast hole broadening effects[41, 44]. We note here that rate constants extracted from the global analysis are approximately equal for all reported solvents, where one might expect a range in this relaxation time if it purely had a solvent component. In THF and DCM, the decay of EADS2 is assigned to the ET rate, since EADS2 in these solvents have spectral profiles that reflect EADS3 in the PhCN and toluene cases.

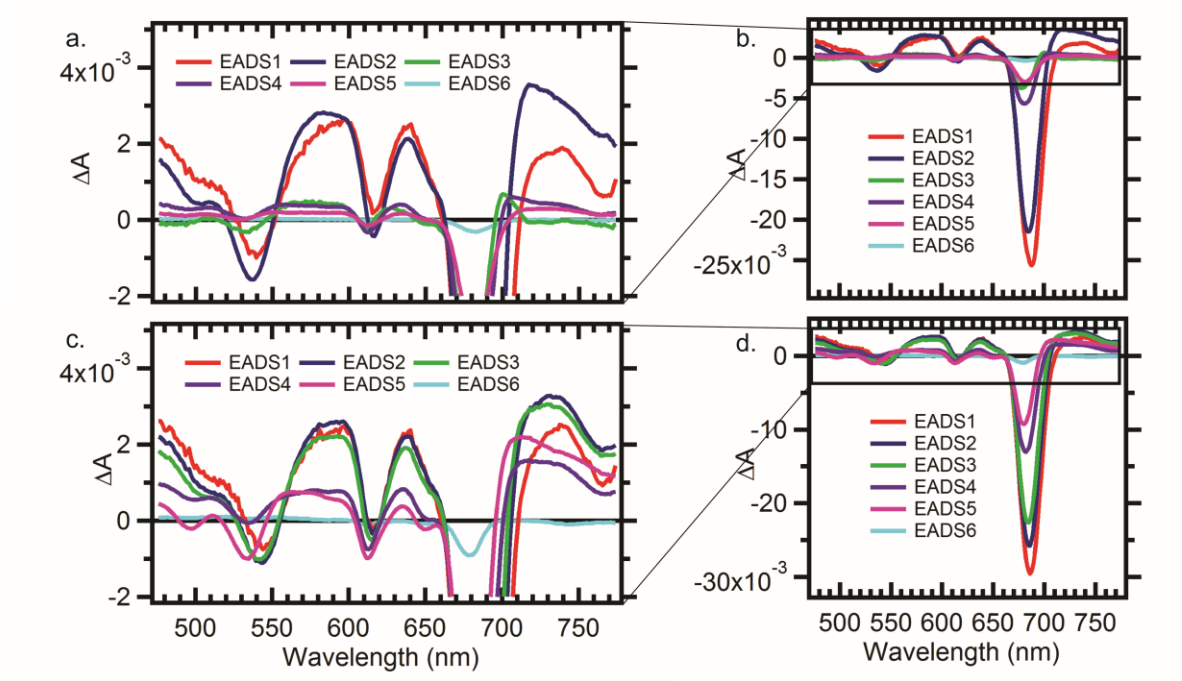

Figure 5. Global analysis EADS using six states and six rates for a,b. ZnPc-PDI in DCM and c,d. ZnPc-PDI in toluene upon photoexcitation at 685 nm. Figures 5a, c. are magnified plots of the ESA structure of the EADS in DCM and toluene, respectively.

In all solvents, we see that the EADS4 decay rate is greater than that of EADS5, and that beside a decrease in amplitude of the GSB feature of ZnPc, the ESA and GSB feature of the PDI remain with approximately the same amplitude and slightly blueshifted, which would be in accordance with a vibrational cooling and solvent relaxation to the bottom of the $ZnPc^{+}$-PDI^{-} free energy surface. In the case of THF and DCM, this cascade of relaxation begins at EADS3, since in these cases their EADS already display greatly reduced ZnPc moiety SE signal. We assign the precursor of the bET to the EADS which decays into a spectrum without the GSB of the PDI, which corresponds to EADS5 and 6, respectively. By assigning the decay of EADS5 to the recombination of the $ZnPc^{+}$-PDI^{-} to the ground state, we are implicitly assuming the CS state transient spectra, leading us to a straightforward comparisons with spectra taken via spectro-electrochemistry or transient spectra taken with the same chromophores, but in other weakly coupled systems[26]. We assign EADS6 to a minor population of photoexcited ZnPc monomer in the dyad solution, which decays on a timescale out of the range of the experiment, which is in accordance with a long lifetime ZnPc triplet state.

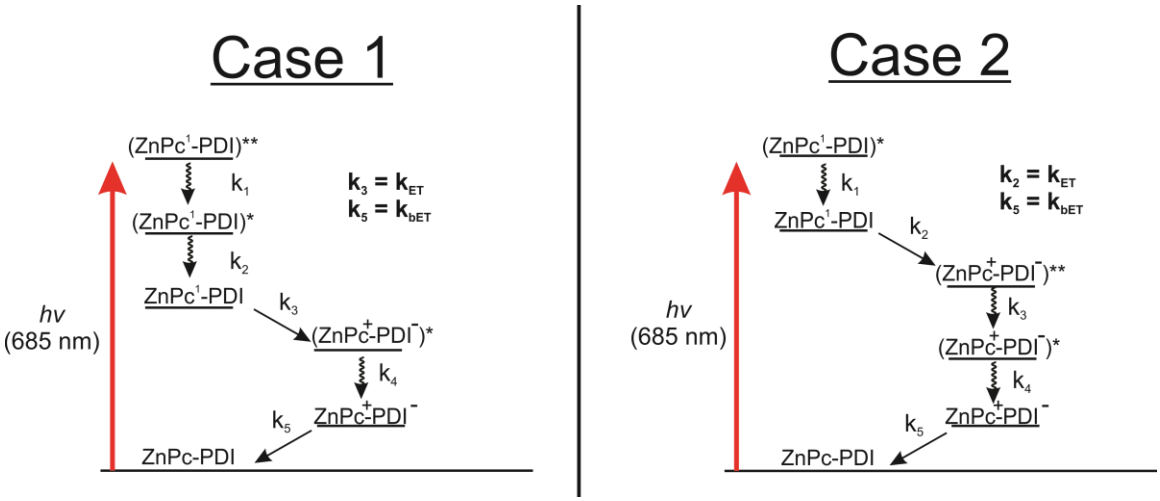

Figure 6. Kinetic scheme derived from global analysis of ZnPc-PDI photoexcitation at 685 nm, where in case 1 the dyad is in toluene or PhCN solution and in case 2 the dyad is in DCM or THF solution. Asterisks (*) denote vibrationally hot or higher energy solvent configurations about the excited state, for which the wavy arrows denote the cooling or solvation process.

Table 2. Contextualizing ET and bET rates with kinetic and energetic parameters

solvent	k_{ET} (ps^{-1})	τ_d^{-1} (ps^{-1})[c]	$-\Delta G_{CS}$ (eV)[d]	k_{bET} (ps^{-1})[e]	$-\Delta G_{CR}$ (eV)	$\lambda_{solvent}$ (eV)[f]
DCM	0.40[a]	0.45[45]	1.01	0.014	0.79	0.74

THF	0.23[a]	0.25[46]	0.98[28]	0.0096	0.82	0.72
PhCN	0.21[b]	0.21[47]	1.16	0.017	0.64	0.75
Tol	0.09[b]	0.18[47]	0.42	0.0009	1.38	0.05

Taken from the values of the decay constants of a. EADS2 b. and EADS3 c. Taken from literature values of longitudinal dielectric relaxation time d. Calculated from the Weller equation (S14) e. Taken from the values of the decay constants of EADS5 f. Calculated from Marcus expression for reorganization energy (S15).

As noted in Table 2, the rates of the forward ET in all solvents deviate very little from the inverse of the solvent dielectric relaxation time, τ_d^{-1}. This observation is reminiscent of the Bixon-Jortner model for solvent-controlled barrierless ET, where in the adiabatic limit the rate of electron transfer is imposed by the solvent relaxation time[48]. This solvent-response dependence is quite precedent in the literature, particularly in twisted-intramolecular charge transfer (TICT) systems[49] and other similar systems[50-51]. We find the best agreement between k_{ET} and $1/\tau_d$ in the polar solvents, while in toluene we observe that the rate of electron transfer is slightly slower than the rate of solvent relaxation.

Upon calculation of the solvent reorganization energy $\lambda_{solvent}$, we note that that the magnitude of the free energy of charge separation, ΔG_{CS}, calculated from cyclic voltammetry measurements[28], is greater than that of the reorganization energy for each solvent tested. This formally sets the ET reaction in the Marcus inverted region. To reconcile the kinetic trend with the solvent relaxation and reorganization energy, we interpret the ET reaction in the Bixon-Jortner model and include high-frequency vibrational modes according to the following equations:

$$k_{ET} = \sum_0^n \frac{k_{NA}^n}{(1+\mathcal{H}_A^n)} \tag{5}$$

$$k_{NA}^n = \frac{2\pi V_n^2}{\hbar\sqrt{4\pi\lambda_{solvent}k_BT}} \exp\left(-\frac{\Delta G_{CS}+\lambda_{solvent}+nh\nu}{4\pi\lambda_{solvent}k_BT}\right) \tag{6}$$

$$\mathcal{H}_A^n = 2V_n^2\langle\tau_d\rangle/\hbar\lambda_{solvent}$$

Equations (5,6) describe the measured ET rate within the framework of the nonadiabatic electron transfer rates, k_{NA}, to vibrationally-hot D^+-A^-, where n is the number of quanta of an arbitrary high-frequency vibrational mode ν. While the coupling between the D*-A and D^+-A^- state, V, in this framework is still electronic in nature, V_n designates a weighting term proportional to the Franck-Condon factor between the lowest vibrationally excited state of the reactant state and the n-th vibrationally excited product state. In the context of the PDI-ZnPc dyad presented here, the high frequency modes can come from either the donor ZnPc or acceptor PDI moieties. The adiabaticity parameter, $\mathcal{H}_A^n$, contributes the dependence on τ_d for cases in which $\mathcal{H}_A^n \gg 1$. We find that using a generalized high frequency mode (ν = 1000 cm^{-1}, 0.12 eV), there is a series of relevant values of n such that a near-barrierless condition is reached for each solvent case, ranging from n = 2 to 4. The toluene case particularly deviates from the polar solvents in the trend that k_{ET} is similar in value to τ_d^{-1} possibly due to its much smaller reorganization energy at the limit of large adiabaticity.

The rates of deactivation of $ZnPc^{+}$-PDI^{-} is sufficiently described by Marcus theory, since the CS state returns back down to the ground state via a back-electron transfer (bET) to form the singlet ground state of both chromophores[52]. In this case, we can evaluate the different bET rates in the various solvents by using the energetic arguments in terms of free energy difference to explain whether the reactions were in the Marcus normal or inverted regions, where the ΔG energy difference to be considered is the one between the CS state and the ground state, noted as ΔG_{CR} in Table 2. By looking at the energetics in Table 2 for toluene, we note that the magnitude of ΔG_{CR} is much greater than the reorganization energy in this solvent, placing the bET deep into the Marcus inverted region—and indeed, we see the slowest EADS5 decay rate in toluene. We suggest by screening arguments that the CS states in DCM and THF should be lower in energy relative to the CS state in toluene, so that if the bET in toluene is in the inverted region, then the bET in DCM and THF will be energetically lower in the inverted region. This hypothesis is supported by the fact that the decay rates associated with EADS5 have higher values in DCM and THF than in toluene, as well as the results from both the Rehm-Weller calculations and reorganization energy calculations. As further support of the assignment of the bET to a Marcus-type mechanism, we note that the reorganization energy in the case of $ZnPc^{+}$-PDI^{-} in PhCN is sufficiently large to place the recombination to the ground state in the normal regime, and appropriately its deactivation rate is the greatest among the solvents tested.

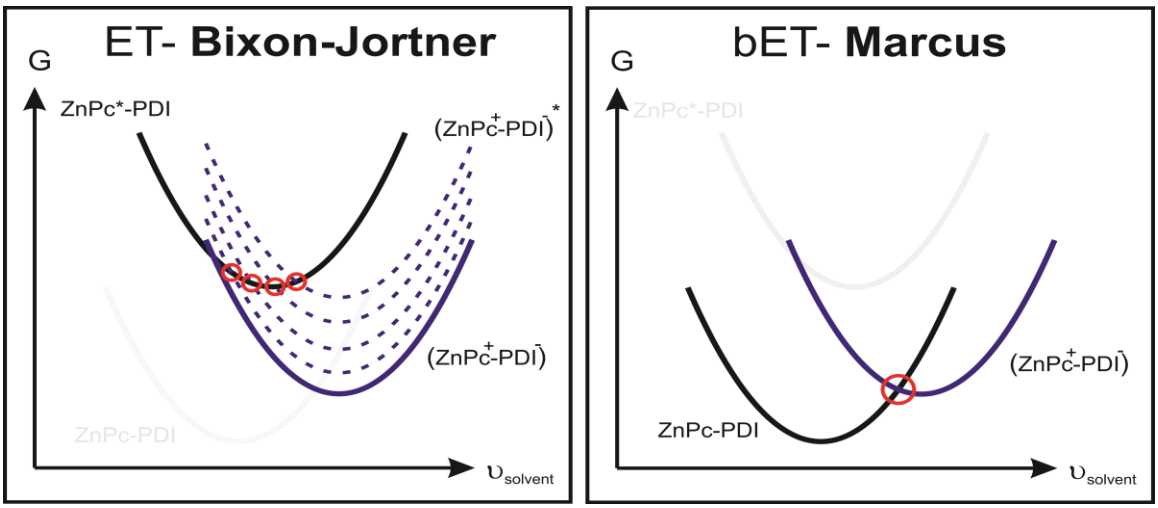

Figure 7. A graphical representation of the proposed arrangement of free energy surfaces of the $ZnPc^{+}$-PDI^{-} species. The figure on the left depicts an electron transfer in the near-barrierless regime to high frequency vibrational modes on the product free energy surface corresponding to the forward ET, while the figure on the right depicts the recombinative back electron transfer according to classical Marcus theory.

5. Conclusion

In this work, we performed a comprehensive study of the ZnPc-PDI dyad by using a combination of solvent variation and ultrafast pump-probe spectroscopy to uncover how EET and ET kinetics change in weakly coupled D-A model systems. By tuning the pump pulse to be in resonance with either the PDI or ZnPc moiety's absorption, we time-resolved the excited-state evolution covering the femto-to-picosecond timescale in the two cases. Global analysis allowed us to correlate spectral evolution with the energy and electron transfer to their respective decay constants, allowing for straightforward comparison of the dyads photochemical kinetics between the different solvents.

In the case of EET after photoexcitation at 540 nm, we quantified the EET rates and found that they could not simply be explained solely by the change in the solvent parameters. We proposed instead that the equilibrium configuration of the ZnPc-PDI's constituent chromophores may change depending on dielectric environment or solvent packing. In the 685 nm experiment, we directly induce the ET mechanism. In all the solvents the ET rate trends closely along with the dielectric relaxation time of the solvents used. We interpreted these findings within the Bixon-Jortner ET framework, such that the dyad undergoes solvent-controlled barrierless ET from the reactant free energy surface to a high frequency vibrational mode in the product state. For the bET, we suggest that the relatively high dielectric screening in PhCN brings this electron transfer in the normal region while in toluene, THF, and DCM they are in different locations in the inverted region, which rationalizes the faster decay rate in PhCN. The relatively fast recombination of the CS state in PhCN has been previously reported in similar ET dyads[53-54], for which this work provides an explanation for in terms of Marcus normal region ET.

While varying the solvent in these types of photoinduced ET systems is common in the literature, our work provides insight into both static and dynamic roles played by the solvent in the charge-transfer process by using a set of solvents which span different dielectric relaxation times and dielectric constants, allowing straightforward assignment into ET theories with varying levels of complexity[55-57]. This study overall highlights some of the nuances of non-rigid model DA systems, where not only do we consider the implications of our dyad's adjustable relative moiety orientation depending on interactions with solvent, but that we can also justify and explain its dynamic photochemistry within accepted models of EET and ET.

Supporting information description

Steady-state spectra of PMAMI, ZnPc, and ZnPc-PDI, single wavelength traces of pump-probe spectra after excitation of ZnPc-PDI at 540 nm, global analyses of ZnPc-PDI after photoexcitation at 685 with 5 states and residuals for all fits, and calculations associated with EET modeling and ET energetics.

Author contributions

B.K. and M.M. performed the experiments and analyzed the data. V. F and J. O. synthesized the molecules studied. B.K., M.M., A.S.S and G.D.S. wrote the paper. All authors commented on the manuscript.

Acknowledgements

B.K. would like to acknowledge Dr. Shahnawaz Rather and Dr. Marius Koch for insightful discussions on photoinduced electron transfer as well as Dan Oblinsky, Dr. Ryan Pensack, and Dr. Evgeny Ostroumov for guidance in performing global analysis.

Funding acknowledgement

This research was financially supported by the Spanish Ministry of Economy and Competitiveness (Mineco) of Spain (CTQ2014-55798-R) and the Division of Chemical Sciences, Geosciences, and Biosciences, Office of Basic Energy Sciences of the U.S. Department of Energy through Grant No. DE-SC0015429. M.M. acknowledges financial support by European Community (H2020 Marie Skłodowska-Curie Actions), Project No. 655059.

References

1. Farver, O.; Pecht, I., *Copper proteins as model systems for investigating intramolecular electron transfer processes*. 1999; Vol. 107, p 555-589.
2. Guldi, D. M., Fullerene–porphyrin architectures; photosynthetic antenna and reaction center models. *Chemical Society Reviews* **2002,** *31* (1), 22-36.
3. Gust, D.; Moore, T. A., Photosynthetic Model Systems. **1991,** *159*.
4. Gust, D.; Moore, T. A.; Moore, A. L., Molecular mimicry of photosynthetic energy and electron transfer. *Accounts of Chemical Research* **1993,** *26* (4), 198-205.
5. Reid, O. G.; Pensack, R. D.; Song, Y.; Scholes, G. D.; Rumbles, G., Charge photogeneration in neat conjugated polymers. *Chemistry of Materials* **2014,** *26* (1), 561-575.
6. Song, P.; Li, Y.; Ma, F.; Pullerits, T.; Sun, M., Photoinduced Electron Transfer in Organic Solar Cells. *Chem Rec* **2016,** *16* (2), 734-53.
7. Wasielewski, M. R., Photoinduced electron transfer in supramolecular systems for artificial photosynthesis. *Chemical Reviews* **1992,** *92* (3), 435-461.
8. Bottari, G.; Trukhina, O.; Ince, M.; Torres, T., Towards artificial photosynthesis: Supramolecular, donor–acceptor, porphyrin- and phthalocyanine/carbon nanostructure ensembles. *Coordination Chemistry Reviews* **2012,** *256* (21-22), 2453-2477.
9. Warman, J. J. M.; De Haas, M. P.; Verhoeven, J. W.; Paddon-Row, M. N.; Yerhoeven, J. W., *Photoinduced Electron Transfer within Donor-□Spacer-□Acceptor Molecular Assemblies Studied by Time-□Resolved Microwave Conductivity*. 1999; Vol. 106, p 571-601.
10. Bottari, G.; de la Torre, G.; Guldi, D. M.; Torres, T., Covalent and noncovalent phthalocyanine-carbon nanostructure systems: synthesis, photoinduced electron transfer, and application to molecular photovoltaics. *Chem Rev* **2010,** *110* (11), 6768-816.
11. Harriman, A.; Sauvage, J.-P., A strategy for constructing photosynthetic models: porphyrin-containing modules assembled around transition metals. *Chemical Society Reviews* **1996,** *25* (1), 41.
12. D'Souza, F.; Ito, O., Supramolecular donor-acceptor hybrids of porphyrins/phthalocyanines with fullerenes/carbon nanotubes: electron transfer, sensing, switching, and catalytic applications. *Chem Commun (Camb)* **2009,** (33), 4913-28.

13. Claessens, C. G.; Hahn, U.; Torres, T., Phthalocyanines: From outstanding electronic properties to emerging applications. *Chemical Record* **2008,** *8* (2), 75-97.
14. Zhan, X.; Facchetti, A.; Barlow, S.; Marks, T. J.; Ratner, M. A.; Wasielewski, M. R.; Marder, S. R., Rylene and related diimides for organic electronics. *Advanced Materials* **2011,** *23* (2), 268-284.
15. Wurthner, F., Perylene bisimide dyes as versatile building blocks for functional supramolecular architectures. *Chem Commun (Camb)* **2004,** (14), 1564-79.
16. Würthner, F.; Saha-Möller, C. R.; Fimmel, B.; Ogi, S.; Leowanawat, P.; Schmidt, D., Perylene Bisimide Dye Assemblies as Archetype Functional Supramolecular Materials. *Chemical Reviews* **2016,** *116* (3), 962-1052.
17. McHugh, A. J.; Gouterman, M.; Weiss, C., Porphyrins XXIV. Energy, oscillator strength, and Zeeman splitting calculations (SCMO-CI) for phthalocyanine, porphyrins, and related ring systems. *Theoretica Chimica Acta* **1972,** *24* (4), 346-370.
18. Zhong, Y.; Kumar, B.; Oh, S.; Trinh, M. T.; Wu, Y.; Elbert, K.; Li, P.; Zhu, X.; Xiao, S.; Ng, F.; Steigerwald, M. L.; Nuckolls, C., Helical ribbons for molecular electronics. *Journal of the American Chemical Society* **2014,** *136* (22), 8122-8130.
19. Fernández-Lázaro, F.; Zink-Lorre, N.; Sastre-Santos, Á., Perylenediimides as non-fullerene acceptors in bulk-heterojunction solar cells (BHJSCs). *J. Mater. Chem. A* **2016,** *4* (24), 9336-9346.
20. Gregory, P., Industrial applications of phthalocyanines. *Journal of Porphyrins and Phthalocyanines (JPP)* **2000,** *04* (04), 432-437.
21. Sung, J.; Nowak-Król, A.; Schlosser, F.; Fimmel, B.; Kim, W.; Kim, D.; Würthner, F., Direct Observation of Excimer-Mediated Intramolecular Electron Transfer in a Cofacially Stacked Perylene Bisimide Pair. *Journal of the American Chemical Society* **2016,** (Dcm), jacs.6b04591-jacs.6b04591.
22. Hu, J.-y.; Paudel, A.; Seto, N.; Feng, X.; Era, M., Marcrocyclic Dyads Based on C60 and Perylenediimides Connected by Click Chemistry. **2014,** *201* (MAY), 1-11.
23. Fernandez-Ariza, J.; Calderon, R. M. K.; Rodriguez-Morgade, M. S.; Guldi, D. M.; Torres, T., Phthalocyanine-Perylenediimide Cart Wheels. *Journal of the American Chemical Society* **2016**, jacs.6b07432-jacs.6b07432.
24. Berera, R.; Herrero, C.; van Stokkum, I. H. M.; Vengris, M.; Kodis, G.; Palacios, R. E.; van Amerongen, H.; van Grondelle, R.; Gust, D.; Moore, T. A.; Moore, A. L.; Kennis, J. T. M., A simple artificial light-harvesting dyad as a model for excess energy dissipation in oxygenic photosynthesis. *Proceedings of the National Academy of Sciences* **2006,** *103* (14), 5343-5348.
25. Marı´a del Rosario Benites, T. E. J., Steven Weghorn, Lianhe Yu,; Polisetti Dharma Rao, J. R. D., Sung Ik Yang, Christine Kirmaier,; David F. Bocian, D. H., and Jonathan S. Lindsey, Synthesis and properties of weakly coupled dendrimeric

multiporphyrin light-harvesting arrays and hole-storage reservoirs. *Journal of Materials Chemistry* **2002,** *12* (1), 65-80.
26. Fukuzumi, S.; Ohkubo, K.; Ortiz, J.; Gutierrez, A. M.; Fernandez-Lazaro, F.; Sastre-Santos, A., Formation of a long-lived charge-separated state of a zinc phthalocyanine-perylenediimide dyad by complexation with magnesium ion. *Chem Commun (Camb)* **2005,** (30), 3814-6.
27. Fukuzumi, S.; Ohkubo, K.; Ortiz, J.; Gutierrez, A. M.; Fernandez-Lazaro, F.; Sastre-Santos, A., Control of photoinduced electron transfer in zinc phthalocyanine-perylenediimide dyad and triad by the magnesium ion. *J Phys Chem A* **2008,** *112* (43), 10744-52.
28. Blas-Ferrando, V. M.; Ortiz, J.; Bouissane, L.; Ohkubo, K.; Fukuzumi, S.; Fernández-Lázaro, F.; Sastre-Santos, Á., Rational design of a phthalocyanine–perylenediimide dyad with a long-lived charge-separated state. *Chemical Communications* **2012,** *48* (50), 6241-6241.
29. Marcus, R. A.; Sutin, N., Electron transfers in chemistry and biology. *BBA Reviews On Bioenergetics* **1985,** *811* (3), 265-322.

30. Olaya-Castro, A.; Scholes, G. D., Energy transfer from Forster-Dexter theory to quantum coherent light-harvesting. *International Reviews In Physical Chemistry* **2011,** *30* (1), 49-77.
31. Follana-Berná, J.; Inan, D.; Blas-Ferrando, V. M.; Gorczak, N.; Ortiz, J.; Manjón, F.; Fernández-Lázaro, F.; Grozema, F. C.; Sastre-Santos, Á., Synthesis and Photophysical Properties of Conjugated and Nonconjugated Phthalocyanine–Perylenediimide Systems. *The Journal of Physical Chemistry C* **2016**.
32. Bixon, M.; Jortner, J., *Electron Transfer: From Isolated Molecules to Biomolecules*. 1999; Vol. 106, p 35-203.
33. Pensack, R. D.; Ostroumov, E. E.; Tilley, A. J.; Mazza, S.; Grieco, C.; Thorley, K. J.; Asbury, J. B.; Seferos, D. S.; Anthony, J. E.; Scholes, G. D., Observation of Two Triplet-Pair Intermediates in Singlet Exciton Fission. *J Phys Chem Lett* **2016,** *7* (13), 2370-5.
34. Van Stokkum, I. H. M.; Larsen, D. S.; Van Grondelle, R., Global and target analysis of time-resolved spectra. *Biochimica et Biophysica Acta - Bioenergetics* **2004,** *1657* (2-3), 82-104.
35. Snellenburg, J. J.; Laptenok, S. P.; Seger, R.; Mullen, K. M.; Stokkum, I. H. M. v., Glotaran: AJava-Based Graphical User Interface for theRPackageTIMP. *Journal of Statistical Software* **2012,** *49* (3).
36. Ambrosek, D.; Marciniak, H.; Lochbrunner, S.; Tatchen, J.; Li, X. Q.; Wurthner, F.; Kuhn, O., Photophysical and quantum chemical study on a J-aggregate forming perylene bisimide monomer. *Phys Chem Chem Phys* **2011,** *13* (39), 17649-57.
37. Ford, W. E.; Kamat, P. V., Photochemistry of 3,4,9,10-perylenetetracarboxylic dianhydride dyes. 3. Singlet and triplet excited-state properties of the bis(2,5-di-tert-butylphenyl)imide derivative. *The Journal of Physical Chemistry* **1987,** *91* (25), 6373-6380.
38. Mack, J.; Stone, J.; Nyokong, T., Trends in the TD-DFT calculations of porphyrin and phthalocyanine analogs. *Journal of Porphyrins and Phthalocyanines* **2014,** *18* (08n09), 630-641.
39. Cott, T. V.; Rose, J., Magnetic circular dichroism and absorption spectrum of zinc phthalocyanine in an argon matrix between 14700 and 74000 cm-1. *The Journal of Physical Chemistry* **1989,** *93*, 2999-3011.
40. Ogunsipe, A.; Maree, D.; Nyokong, T., Solvent effects on the photochemical and fluorescence properties of zinc phthalocyanine derivatives. *Journal of Molecular Structure* **2003,** *650* (1-3), 131-140.
41. Savolainen, J.; van der Linden, D.; Dijkhuizen, N.; Herek, J. L., Characterizing the functional dynamics of zinc phthalocyanine from femtoseconds to nanoseconds. *Journal of Photochemistry and Photobiology A: Chemistry* **2008,** *196* (1), 99-105.
42. Rao, S. V.; Rao, D. N., Excited state dynamics in phthalocyanines studied using degenerate four wave mixing with incoherent light. *Journal of Porphyrins and Phthalocyanines* **2002,** *06* (03), 233-237.
43. Chenu, A.; Scholes, G. D., Coherence in energy transfer and photosynthesis. *Annual review of physical chemistry* **2015,** *66* (August), 69-96.
44. Middendorf, T. R.; Mazzola, L. T.; Gaul, D. F.; Schenck, C. C.; Boxer, S. G., Photochemical hole-burning spectroscopy of a photosynthetic reaction center mutant with altered charge separation kinetics: properties and decay of the initially excited state. *The Journal of Physical Chemistry* **1991,** *95* (24), 10142-10151.
45. Hunger, J.; Stoppa, A.; Thoman, A.; Walther, M.; Buchner, R., Broadband dielectric response of dichloromethane. *Chemical Physics Letters* **2009,** *471* (1-3), 85-91.
46. Kumbharkhane, A. C.; Helambe, S. N.; Lokhande, M. P.; Doraiswamy, S.; Mehrotra, S. C., Structural study of aqueous solutions of tetrahydrofuran and acetone mixtures using dielectric relaxation technique. *Pramana* **1996,** *46* (2), 91-98.
47. Walker, G. C.; Aakesson, E.; Johnson, A. E.; Levinger, N. E.; Barbara, P. F., Interplay of solvent motion and vibrational excitation in electron-transfer kinetics: experiment and theory. *The Journal of Physical Chemistry* **1992,** *96* (9), 3728-3736.
48. Rips, I.; Jortner, J., Activationless solvent-controlled electron transfer. *The Journal of Chemical Physics* **1988,** *88* (2), 818.

49. Kosower, E. M.; Huppert, D., Excited State Electron and Proton Transfers. *Annual Review of Physical Chemistry* **1986,** *37* (1), 127-156.
50. Simon, J. D.; Su, S. G., Dynamic solvent effects on intramolecular electron-transfer reactions: fluctuation time scales and population decays. *The Journal of Physical Chemistry* **1988,** *92* (9), 2395-2397.
51. Kahlow, M. A.; Kang, T. J.; Barbara, P. F., Transient solvation of polar dye molecules in polar aprotic solvents. *The Journal of Chemical Physics* **1988,** *88* (4), 2372.
52. Bredas, J. L.; Beljonne, D.; Coropceanu, V.; Cornil, J., Charge-transfer and energy-transfer processes in pi-conjugated oligomers and polymers: a molecular picture. *Chem Rev* **2004,** *104* (11), 4971-5004.
53. Stranius, K.; Iashin, V.; Nikkonen, T.; Muuronen, M.; Helaja, J.; Tkachenko, N., Effect of mutual position of electron donor and acceptor on photoinduced electron transfer in supramolecular chlorophyll-fullerene dyads. *J Phys Chem A* **2014,** *118* (8), 1420-9.
54. Robotham, B.; Lastman, K. A.; Langford, S. J.; Ghiggino, K. P., Ultrafast electron transfer in a porphyrin-amino naphthalene diimide dyad. *Journal of Photochemistry and Photobiology A: Chemistry* **2013,** *251*, 167-174.
55. Imahori, H.; Hagiwara, K.; Aoki, M.; Akiyama, T.; Taniguchi, S.; Okada, T.; Shirakawa, M.; Sakata, Y., Linkage and Solvent Dependence of Photoinduced Electron Transfer in Zincporphyrin-C60Dyads. *Journal of the American Chemical Society* **1996,** *118* (47), 11771-11782.
56. Duvva, N.; Sudhakar, K.; Badgurjar, D.; Chitta, R.; Giribabu, L., Spacer controlled photo-induced intramolecular electron transfer in a series of phenothiazine-boron dipyrromethene donor–acceptor dyads. *Journal of Photochemistry and Photobiology A: Chemistry* **2015,** *312*, 8-19.
57. Janice M. Degraziano, A. N. M., Paul A. Liddell, Lori Noss, John P. Sumida, Gibert R. Seely, Jeffrey E. Lewis, Ana L. Moore, Thomas A. Moore, Devens Gust, Solvent dependence of photoinduced electron transfer in porphyrin dyads. *New Journal of Chemistry* **1996,** *20* (7-8), 839-851.